SCIENTIFIC REPORTS

OPEN

SUBJECT AREAS:
CANCER THERAPY
CANCER IMAGING
NANOMEDICINE
CHEMICAL BIOLOGY

Received
27 February 2013

Accepted
24 May 2013

Published
17 June 2013

Correspondence and requests for materials should be addressed to H.H.Y. (hhyang@fio.org.cn); D.R.C. (dairongcao@yahoo.com.cn) or W.R.S. (swenrong@163.com)

Topological insulator bismuth selenide as a theranostic platform for simultaneous cancer imaging and therapy

Juan Li[1], Fei Jiang[2], Bo Yang[2], Xiao-Rong Song[1], Yan Liu[3], Huang-Hao Yang[1], Dai-Rong Cao[2], Wen-Rong Shi[3] & Guo-Nan Chen[1]

[1]The Key Lab of Analysis and Detection Technology for Food Safety of the MOE, Fujian Provincial Key Laboratory of Analysis and Detection Technology for Food Safety, College of Chemistry and Chemical Engineering, Fuzhou University, Fuzhou 350002, P. R. China, [2]Department of Radiology, First Affiliated Hospital of Fujian Medical University, Fuzhou 350005, P. R. China, [3]College of Integrated Traditional Chinese and Western Medicine, Fujian University of Traditional Chinese Medicine, Fuzhou 350108, P. R. China.

Employing theranostic nanoparticles, which combine both therapeutic and diagnostic capabilities in one dose, has promise to propel the biomedical field toward personalized medicine. Here we investigate the theranostic properties of topological insulator bismuth selenide (Bi_2Se_3) in *in vivo* and *in vitro* system for the first time. We show that Bi_2Se_3 nanoplates can absorb near-infrared (NIR) laser light and effectively convert laser energy into heat. Such photothermal conversion property may be due to the unique physical properties of topological insulators. Furthermore, localized and irreversible photothermal ablation of tumors in the mouse model is successfully achieved by using Bi_2Se_3 nanoplates and NIR laser irradiation. In addition, we also demonstrate that Bi_2Se_3 nanoplates exhibit strong X-ray attenuation and can be utilized for enhanced X-ray computed tomography imaging of tumor tissue in vivo. This study highlights Bi_2Se_3 nanoplates could serve as a promising platform for cancer diagnosis and therapy.

Cancer is a term used for diseases in which abnormal cells divide without control and are able to invade other tissues. According to the World Health Organization, cancer is a leading cause of death and accounted for 7.6 million deaths (around 13% of all deaths) in 2008. This number is expected to rise to 12 million by 2030[1]. The increase in cancer deaths is signaling the pressing need for newer, even more effective diagnostics and therapies. Recently, "theranostics", which incorporate both therapy and diagnosis, are attracting significant attention[2]. The integration of diagnostic imaging capability with therapeutic interventions is critical in addressing the challenges of cancer heterogeneity and adaptation. Therefore, theranostic agents have attracted enormous interest in cancer diagnosis and treatment in recent years.

Albeit substantial progress was accomplished, conventional diagnostic and therapeutic agents, such as iodinated contrast agent, radio-labeled biomolecules, or chemotherapy drugs, are often limited by short blood circulation times and nonspecific biodistribution[3]. The emergence of nanomaterials offers new opportunities for advanced diagnostics and therapeutics. Nanomaterials provide several potential advantages over conventional agents, including extension of circulating half-life, passive accumulation at tumor sites due to the enhanced permeability and retention (EPR) effect, reduced toxicity and integration of multiple diverse functions in a single complex[3]. Up to now, several nanomaterials have acted as nanotheranostic agents[4–7], such as magnetic nanoparticles[8–10], carbon nanotubes[11,12], gold-based nanostructures[13–15] and nanoshells-based nanoparticles[3,16]. Although impressive advances have been made in nanotheranostic agents, the types of nanomaterials with efficient diagnostic imaging and therapeutic capabilities simultaneously are limited. Therefore, there is still a great demand for developing new nanomaterials for the diagnosis and treatment of different cancers.

Topological insulators are a new class of quantum matter for which their bulk phases are ordinary insulators but possess robust, nontrivial, and conducting surface or boundary states with nondegenerate spins[17]. Beyond the inherent importance of exploring complex phases of quantum matter, topological insulators are of great interest for device applications involving quantum computing and photonics. For their special characteristics, topological insulators have become the rising star in physics and provided challenges and opportunities for chemistry and material science[18]. Bismuth selenide (Bi_2Se_3) is theoretically predicted and experimentally observed to be a three-dimensional (3D) topological insulator with a single Dirac cone[19]. Bi_2Se_3 has attracted great attention in physics

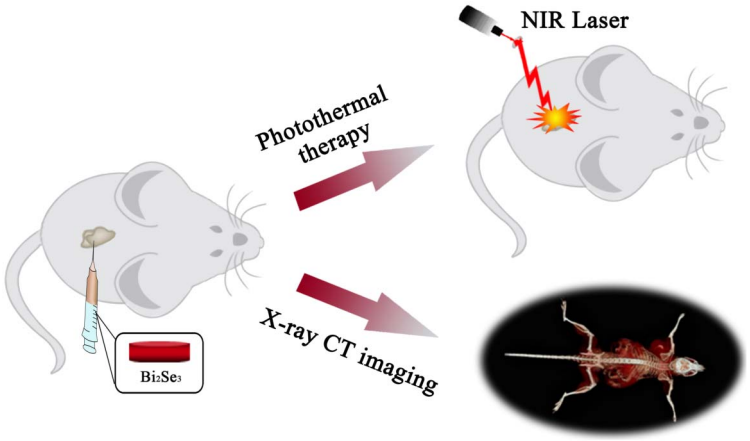

Figure 1 | Schematic representation of topological insulator bismuth selenide as a theranostic platform. Bismuth selenide is able to perform for simultaneous X-ray CT imaging and photothermal therapy.

and chemistry because of its remarkable thermoelectric[20], optical[21] and photoelectric properties[22]. Although, the synthesis and investigation of the physical properties of Bi_2Se_3 have been undertaken, little has been done to explore Bi_2Se_3 in biomedical fields. Bi_2Se_3 is composed of bismuth (Bi) and selenium (Se). Bi is an environmentally friendly element and has a long history of use as a therapeutic agent with low toxicity[23]. Furthermore, Bi is an attractive element for X-ray contrast agents due to its high atomic number (Z = 83) and well-known biological tolerance[24]. Recently, some Bi-based nanomaterials have been explored as high contrast, long-circulating, low-toxicity X-ray contrast agents[25–27]. The other component is Se, which is an essential trace element for human. The recommended dietary allowance of Se is 55 μg per day for healthy human adults[28]. Meanwhile, Se also plays important biological roles through the selenoproteins, which helps protect tissues and membranes from oxidative stress and controls cell redox status[29]. In addition, accumulating evidence indicates that Se has benefits in reducing the risk of cancer incidence and mortality in many cancer types, and specifically in liver, prostate and lung cancers[30]. Therefore, Bi_2Se_3 is presumed to be biocompatible and holds great potential in biomedical fields.

Here we investigate the theranostic properties of Bi_2Se_3 nanoplates in *in vivo* and *in vitro* system for the first time (Fig. 1). We show that Bi_2Se_3 nanoplates can absorb NIR laser light and effectively convert laser energy into heat. The photothermal conversion properties of topological insulators have not been reported so far, although many excellent physical properties of topological insulators have been extensively investigated. Besides, Bi_2Se_3 nanoplates also exhibit strong X-ray attenuation for in vivo X-ray computed tomography (CT) imaging. Therefore, topological insulator Bi_2Se_3 holds promise as a novel theranostic platform.

Results

Synthesis and characterization of Bi_2Se_3 nanoplates. Bi_2Se_3 nanoplates were prepared by a simple synthetic route and coated with polyvinylpyrrolidone (PVP)[31]. PVP is a biodegradable and water-soluble biocompatible polymer and is frequently employed as binding, dispersing and stabilizing agent in pharmaceutical tablets and injectables[32]. Moreover, PVP has also been used to stabilize a variety of nanoparticles to expand their biological applicability[25,33,34]. The synthesized Bi_2Se_3 nanoplates showed relatively uniform sizes with an average diameter of about 90 nm (Fig. 2a) based on transmission electron microscope (TEM) images. In addition, the as-prepared Bi_2Se_3 has a layered structure based on AFM analysis. The thickness of the outer layer was about 3.9 nm and inner layer was about 21.5 nm (Supplementary Fig. S1). The phase analysis of the as-prepared product was determined by powder X-ray

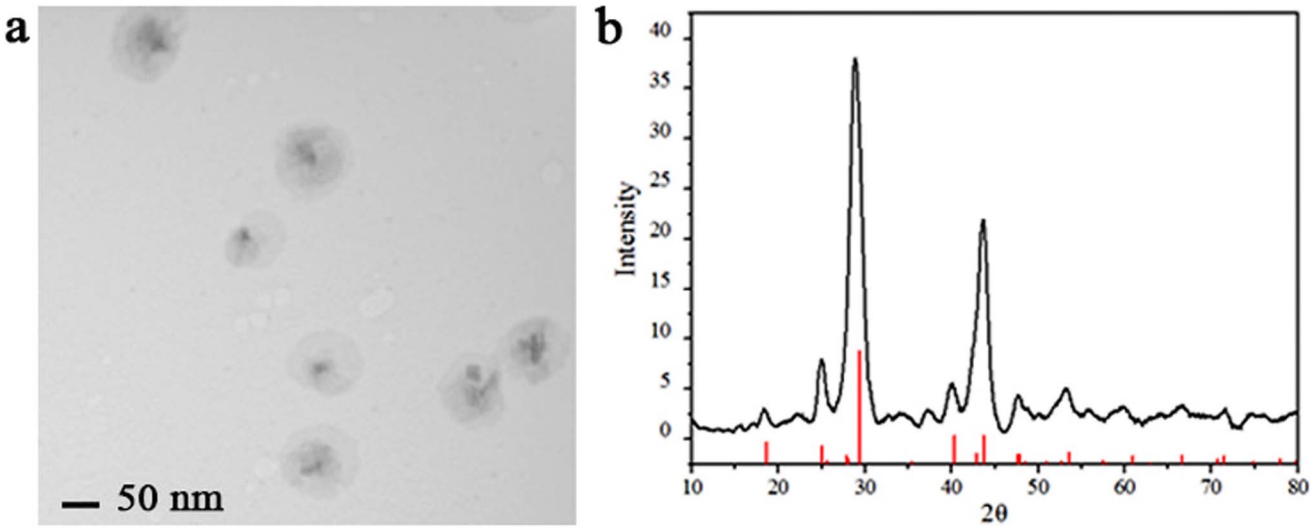

Figure 2 | Characterization of Bi_2Se_3 nanoplates. (a) TEM image and (b) XRD pattern of Bi_2Se_3.

diffraction (XRD) (Fig. 2b). All peaks in the pattern correspond to the reflections of the rhombohedral phase of Bi_2Se_3, which match well with the reported value (JCPDS Card No. 33-0214)[31]. Furthermore, Bi_2Se_3 nanoplates exhibited good dispersion in a range of physiological solutions including saline, cell medium, and serum (Supplementary Fig. S2).

Cytotoxicity and cell internalization of Bi_2Se_3 nanoplates. Prior to using Bi_2Se_3 nanoplates for in vivo imaging and therapy, we tested their cell cytotoxicity using the methyl thiazolyl tetrazolium (MTT) assay at first. Encouragingly, cell viability was not hindered by Bi_2Se_3 nanoplates up to a concentration of 200 $\mu g\ ml^{-1}$ (Fig. 3a). The results suggest that Bi_2Se_3 nanoplates possess low cell cytotoxicity and good biocompatibility. To study the mechanism of the cellular uptake of Bi_2Se_3 nanoplates, we incubated the H22 cells with Bi_2Se_3 nanoplates at 4°C and 37°C, respectively. The uptake efficiency of Bi_2Se_3 nanoplates was investigated using inductively coupled plasma mass spectrometry (ICP-MS). The results shown in Fig. 3b reveal that the cellular uptake of Bi_2Se_3 nanoplates is significantly decreased at 4°C. This result implies cellular uptake of Bi_2Se_3 nanoplates is through an energy-dependent endocytosis[35].

In vitro and in vivo X-ray computed tomography (CT) imaging. Bi_2Se_3 nanoplates hold great promise for CT contrast agents because Bi possesses the large X-ray attenuation coefficient (Bi: 5.74, Au: 5.16, Pt: 4.99, Ta: 4.3 and I: 1.94 cm^2kg^{-1} at 100 keV). In this work, the Hounsfield Units (HU) of Bi_2Se_3 nanoplates was evaluated by a clinical CT. Figure 4a displays the CT images in the range from 0 to 0.0488 mol Bi l^{-1} of Bi_2Se_3 nanoplates. It can be observed that CT signal intensity continuously increases with the increasing of Bi_2Se_3 nanoplates concentrations, resulting in brighter images. To further investigate the CT contrast efficacy, we next compared the X-ray absorption of Bi_2Se_3 to that of Iopamidol in vitro (Fig. 4a). Iopamidol is one of most widely used CT contrast agents in current clinical applications. The results demonstrate that Bi_2Se_3 produces higher contrast than Iopamidol. The HU values increase linearly with concentration for both Bi_2Se_3 and Iopamidol (Fig. 4b). Nevertheless, the HU values of Bi_2Se_3 are higher than that of Iopamidol at equivalent concentrations due to the fact that the attenuation coefficient of Bi is larger than that of iodine (I). Thus, Bi_2Se_3 provides an equivalent contrast at a lower dose compared to the clinical iodinate agent. The reduced dose is highly beneficial because it reduces potential side effects and complications in clinical applications. Furthermore, in vitro CT imaging of H22 cells incubated with different concentrations of Bi_2Se_3 nanoplates was also investigated. Figure 4a (last row) shows the transection CT images of H22 cells with or without incubation of the Bi_2Se_3 nanoplates. It is clear that with the incubated concentration of Bi_2Se_3 nanoplates increasing, H22 cells gradually display brighter CT images.

The excellent in vitro performance of Bi_2Se_3 nanoplates as a potential CT imaging agent encouraged us to pursue their applicability in CT imaging in vivo. The feasibility of Bi_2Se_3 nanoplates as CT contrast agents in vivo was demonstrated by intratumoral injection of Bi_2Se_3 nanoplates. Figure 4c shows the tumor CT images before and after intratumoral injection. The subcutaneous injection site displays a brighter CT signal than other soft tissues, which is attributed to the strong X-ray attenuation induced by Bi. After analysis of the CT values of the tumor area at 30 min and 120 min post-injection, we found that the CT value decreased slightly (627 ± 22.8 versus 545 ± 13.6). It is because with the passage of time, Bi_2Se_3 nanoplates could diffuse in the tumor. Therefore, the CT values of the tumor area would decrease gradually. However, the CT value of tumor area even at 120 min post-injection was still significantly higher than that of the tumor area before injection (545 ± 13.6 versus 85 ± 5.2). As control, the mice were injected with Iopamidol at the central region of the tumor under similar conditions. The inject region showed a white spot with brightness lower than the case of Bi_2Se_3 nanoplates (Supplementary Fig. S3). These results provide strong evidence that Bi_2Se_3 may be a promising contrast agent for CT imaging in future clinical applications.

In vitro and in vivo photothermal therapy. Photothermal therapy (PTT) is a hyperthermia therapeutic approach that employs photoabsorbing agents to burn cancer cells by heat generated from optical energy[36]. Deep penetration and little nonspecific photothermal heating in the near-infrared (NIR) window are due to the transparency and low absorption of light by tissues in this optical window[37]. Compared with traditional cancer therapies such as radiotherapy and chemotherapy, PTT cancer treatment is a minimally invasive or noninvasive technique. In recent years, some NIR light absorbing nanomaterials have been developed for PTT. At present, there are four main types of NIR laser-driven photothermal agents have been extensively developed, resulting in great contributions to progress in PTT. The first type is organic compounds[38–41]. The second type is carbon-based materials, including carbon nanotubes[42–45] and graphene[46–48]. The third type is metal nanostructures, such as Au nanostructures[13–15], palladium nanosheets[49] and chemically exfoliated MoS_2[50]. The last type is copper chalcogenide semiconductors[51–54]. As far as we know, the

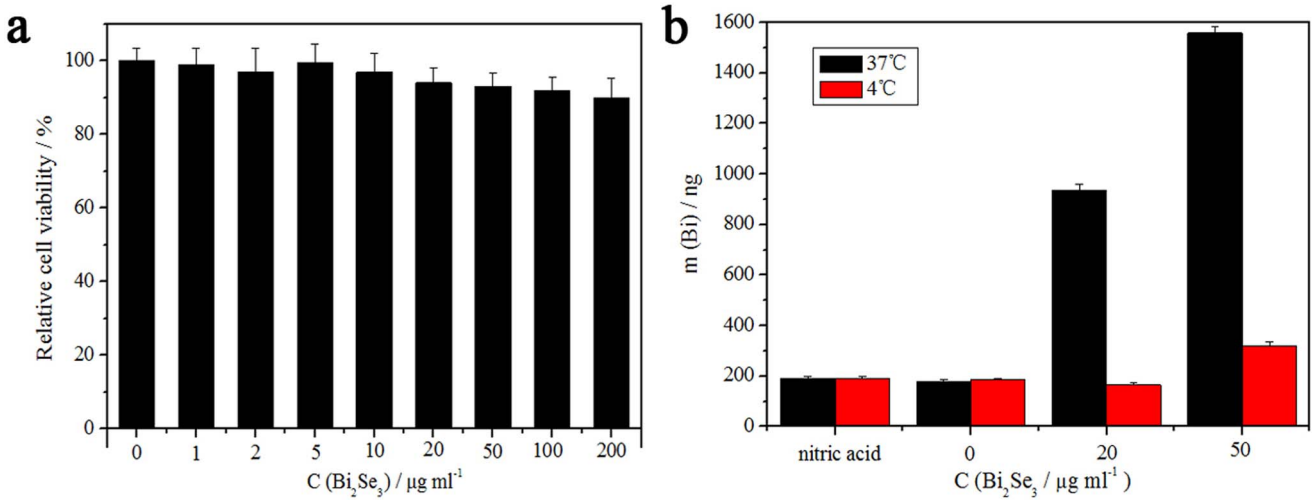

Figure 3 | Cell cytotoxicity and cell internalization of nanoplates. (a) Cell viability of H22 cells after incubation with increased concentration of Bi_2Se_3 nanoplates. (b) ICP-MS results of H22 cells incubated with Bi_2Se_3 nanoplates at 37°C and 4°C. Error bars correspond to mean ± standard deviations.

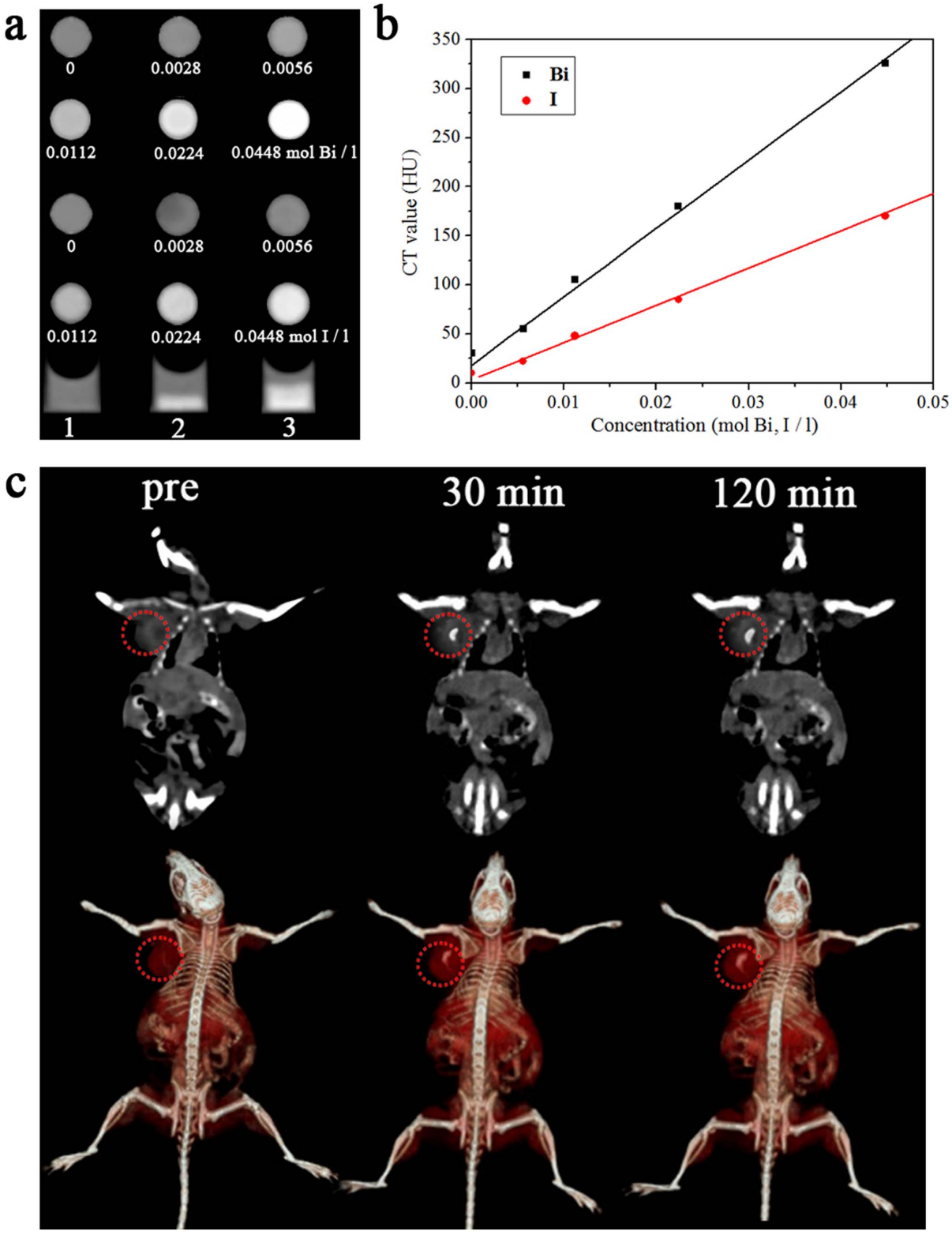

Figure 4 | Results of X-ray CT imaging in vitro and in vivo. (a) In vitro CT images of Bi_2Se_3 nanoplates and Iopamidol with different concentrations. Cell analysis: H22 cells incubated without contrast agent (1), with increased concentration of Bi_2Se_3 nanoplates (0.02 and 0.05 mol Bi l^{-1} for 2 and 3, respectively). (b) CT value (HU) of Bi_2Se_3 nanoplates (■) or Iopamidol (●) as function of the concentration. (c) CT coronal views of a mouse following an intratumoral injection of 100 μl of Bi_2Se_3 nanoplates solution (0.2 mol Bi l^{-1}) (top). The corresponding 3D rendering of in vivo CT images above (bottom). The position of tumor is marked by red circles.

photothermal conversion properties of topological insulators have not been reported so far.

In this work, we demonstrate the Bi_2Se_3 nanoplates display high optical absorption in the NIR range (Supplementary Fig. S4). And they can effectively convert NIR laser radiation into heat. We examined the temperature increase of Bi_2Se_3 nanoplates aqueous solution with various concentrations by the 808 nm laser (Fig. 5a). The temperature of the Bi_2Se_3 nanoplates solution increased rapidly, while

pure water showed a negligible change. The temperature of the solution containing 50 μg ml^{-1} Bi_2Se_3 nanoplates rose from 24.4°C to 50.2°C after 5 min irradiation. We presume that this highly efficient photothermal conversion property may be due to the unique physical properties of topological insulators.

Next, we evaluated in vitro photothermal ablation capacity of Bi_2Se_3 nanoplates with H22 cells. The MTT results showed that H22 cells treated with Bi_2Se_3 nanoplates without laser irradiation remain more than 90% viable at Bi_2Se_3 nanoplates concentrations up to 50 μg ml^{-1}. The cell viability significantly decreased when they were simultaneously treated with Bi_2Se_3 nanoplates and laser irradiation. And only about 25% of H22 cells remained viable at a Bi_2Se_3 nanoplates concentration of 50 μg ml^{-1} (Fig. 5b).

After confirming the photothermal effect of Bi_2Se_3 nanoplates, we attempted in vivo therapeutic examinations against Balb/c mice bearing H22 cancer tumors. After the tumor sizes became approximately 100 mm^3, the mice were divided into four groups (n = 7): (a) sterile water; (b) sterile water + laser; (c) Bi_2Se_3 nanoplates; (d) Bi_2Se_3 nanoplates + laser. For group (d), each mouse was treated with an intratumoral injection of Bi_2Se_3 nanoplates followed by NIR irradiation. One noticeable observation is that there were small black round marks on the skin after treatment. This black mark is a skin burn scar which is a direct evidence of the generation of excessive local heating from Bi_2Se_3 nanoplates by NIR. Under the same irradiation conditions, in contrast, there was no noticeable sign of temperature increase in the mice treated with sterile water followed by NIR irradiation (group b). Another two control groups (a and c) of mice with sterile water or Bi_2Se_3 nanoplates injection were not irradiated.

Tumor sizes were measured every 2 days after the above treatments. Figure 5c shows tumor volume changes of representative mice treated in different groups as a function of time. Tumors that received only Bi_2Se_3 nanoplates injection (group c) or laser irradiation (group b) showed growth rates indistinguishable from control tumors (group a). This result demonstrated that only NIR laser irradiation or Bi_2Se_3 nanoplates injection did not affect the tumor development. In marked contrast, tumors of group (d) were completely eliminated one day after treatment, leaving the original tumor site with black scars which fell off about 1 week later (Fig. 5d). In addition, NIR at power density of 2 W/cm^2 alone did not cause damage to cancer tissues (Supplementary Fig. S5). No tumor regrowth was noted in this treated group over a course of 45 days, after which the study was ended. In addition, the toxicity of the as-prepared Bi_2Se_3 nanoplates was examined in vivo. We did not find any obvious sign of toxic side effects for Bi_2Se_3 nanoplates injected mice within 45 days. Neither death nor significant body weight drop was observed in all experimental groups (Supplementary Fig. S6). Furthermore, major organs of Bi_2Se_3 nanoparticles + laser treated mice (group d) whose tumors were eliminated by the photothermal therapy were collected 45 days after the treatment for histology analysis. No evident tissue damage from the group (d) compared to the control group (a) (Supplementary Fig. S7). Our results suggest that

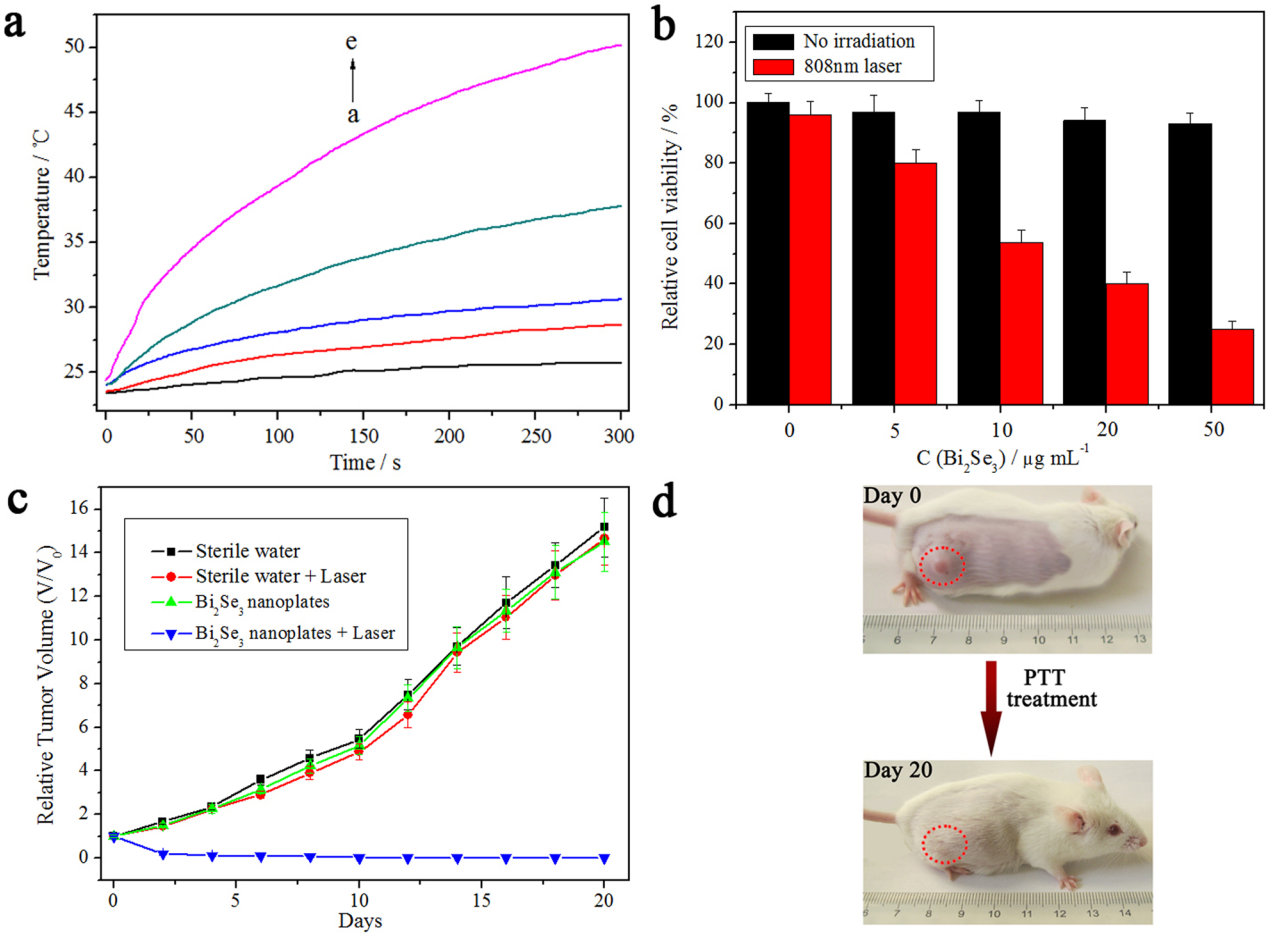

Figure 5 | Photothermal therapy in *in vitro* and *in vivo* system. (a) Photothermal effect of pure water and Bi_2Se_3 nanoplates with different concentrations (a–e: 0, 5, 10, 20, 50 μg ml^{-1}) upon the irradiation of 1 W cm^{-2} 808 nm laser. (b) H22 cell viabilities cultured with Bi_2Se_3 nanoplates at different concentrations with or without laser irradiation. (c) Growth of H22 tumors in different groups of mice after treatment. The relative tumor volumes were normalized to their initial sizes. (d) Representative photos of a Bi_2Se_3 nanoplates-injected mouse at day 0 before PTT treatment and at day 20 after treatment. Error bars correspond to mean ± standard deviations.

Bi_2Se_3 nanoplates may be a powerful agent for in vivo photothermal cancer therapy.

Discussion

The development of new nanomaterials for simultaneous cancer diagnosis and treatment has been receiving great attention in recent years and has now become an important field in medical research. Bi_2Se_3, as a three-dimensional topological insulator, causes wide attention recently. It has been proved that Bi_2Se_3 has many excellent physical properties, such as thermoelectricity and photoelectricity. In present work, we investigate the theranostic properties of Bi_2Se_3 nanoplates in *in vivo* and *in vitro* system. We prove that Bi_2Se_3 nanoplates have the X-ray CT imaging and photothermal therapeutic capabilities simultaneously. On one hand, as an X-ray contrast agent, Bi_2Se_3 nanoplates provide higher contrast efficacy than a clinical iodinate agent. The xenograft tumor model could be imaged using CT after intratumoral administration of Bi_2Se_3 nanoplates. On the other hand, as a photothermal therapeutic agent, Bi_2Se_3 nanoplates can absorb NIR laser and effectively transfer laser energy into heat, then successfully induce complete eradications of solid malignant tumors in mice by hyperthermia. More importantly, the photothermally treated mice were all healthy without toxic effects, abnormal behavior, or recurrence of tumors over a long period of time. Our results clearly indicate that Bi_2Se_3 nanoplates may be a promising platform for simultaneous diagnosis and therapy, and bring novel opportunities in theranostics.

Furthermore, bismuth complexes and selenium complexes have a long history of use as therapeutic agents with low toxicity. In addition, Se has benefits in reducing the risk of cancer incidence and mortality in many cancer types. Therefore, Bi_2Se_3 is presumed to be biocompatible. In our preliminary experiments, the results also prove that Bi_2Se_3 nanoplates have a low toxicity to cells and no observable toxicity in mice.

Although potential applications of Bi_2Se_3 in biomedical fields are shown in this paper, a number of issues demand clarification and further researches. Potential toxicity, the long-term biodistribution and quantitative pharmacokinetics in vivo are extremely important and need to be addressed. On the other hand, the incorporation of tumor targeting ligands with Bi_2Se_3 to achieve active targeting is another interesting issue. These works are underway now in our laboratory and will be communicated in due course.

Methods

Synthetic procedure and characterization of Bi_2Se_3 nanoplates. The Bi_2Se_3 nanoplates were synthesized according to the method published previously[31]. In brief, A reaction batch (100 ml two-neck round-bottom flask) contained ethylene glycol (40 ml), Na_2SeO_3 (99%, Aldrich, 0.06 g), $Bi(NO_3)_3{\cdot}5H_2O$ (99.99%, Aldrich, 0.1125 g), and polyvinylpyrrolidone (PVP) (Mw = 55, 000, Aldrich, 0.25 g) as surfactant. The reaction was triggered by rapid injection of 0.6 ml of hydroxylamine solution (NH_2OH, 50% in H_2O, Aldrich) at 140°C. Then, the reaction mixture turned brown red immediately, which indicated the formation of Bi_2Se_3 nanoplates. The reaction was allowed to process for 10 min for a complete reaction and cooled down to room temperature. The size and morphology of the Bi_2Se_3 nanoplates were characterized using transmission electron microscopy (JEM 1010, JEOL, Japan), at an accelerating voltage of 100 kV. X-ray diffraction (XRD) patterns were obtained by using an X-ray power diffraction meter (D/MAX-3C, Rigaku Co., Japan). UV-vis absorption spectra were measured using a TU-1950 UV-Vis spectrophotometer (Beijing Perkinje General Instrument Co., Ltd., Beijing, China) at room temperature.

Mice and cell lines. Female Balb/c mice (weight about 20 g) were purchased from Shanghai SLAC Laboratory Animal Co. Ltd (Shanghai, China). Animal experiments and animal care were carried out according to protocols approved by the institutional committee for animal care, and also in accordance with the policy of the National Ministry of Health. Murine hepatocarcinoma cell line H22 was purchased from China Centre for Type Culture Collection (CCTCC, Wuhan, China), and cultured according to the guidelines given.

Cellular uptake efficiency and cytotoxicity assessment. In a typical experiment, H22 cells (1×10^4 cells per well) were seeded in 96-well plates and incubated overnight at 37°C in a humidified 5% CO_2 atmosphere. The cells were incubated with 100 μl of varying concentration of Bi_2Se_3 nanoplates prepared above for 24 h at 37°C in the dark under the same conditions. Cell viability was determined by the standard 3-(4,5-dimethylthiazolyl-2)-2,5-diphenyltetrazolium bromide (MTT) (Aldrich) assay. In some cases, cells were collected and digested in HNO_3 (65%) for 24 h, and then diluted in Milli-Q water for ICP-MS (7500CE, Agilent Technologies, USA) analysis.

CT imaging in vitro. The solution of Bi_2Se_3 nanoplates with different concentrations in the range from 0 to 0.0488 mol Bi l^{-1} was directly detected using a 320-detector row scanner (Aquilion ONE; Toshiba Medical Systems, Japan) with the following operating parameters: thickness, 0.5 mm; pitch, 0.5 mm; tube voltage 120 KV; tube current, 50 mA; field of view, 350 mm. CT values were acquired on the same workstation using the software supplied by the manufacturer. Each experiment was carried out in triplicate.

0, 0.02 and 0.05 mol Bi l^{-1} were incubated with H22 cells (1×10^6 cells per well) for 24 h at 37°C under 5% CO_2. After washing with PBS for three times, H22 cells containing Bi_2Se_3 nanoplates in PBS were precipitated at the bottom of the tube for CT imaging.

CT imaging in vivo. 100 μl of 1×10^6 H22 cells (Balb/c background) in PBS was injected into left axilla region of female Balb/c mice. Mice were anesthetized during the CT imaging with 100 μl 20% urethane. CT scanning was performed both before and after intratumoral injection of Bi_2Se_3 nanoplates (100 μl, 0.2 mol Bi l^{-1}). The mice were scanned by CT after 30 min and 120 min post-injection. As control, CT scanning was performed both before and after intratumoral injection of Iopamidol (100 μl, 0.2 mol I l^{-1}). The mice were scanned by CT after 3 min and 60 min post-injection. All CT scans were performed using the above CT system.

In vitro photothermal therapy effects. An optical fiber coupled 808 nm high power diode-laser (Hi-Tech Optoelectronics Co., Ltd. Beijing, China) was used in the experiments. To study the photothermal effect induced by the NIR absorption, 1 ml aqueous solutions containing different concentration (0, 5, 10, 20 and 50 μg ml^{-1}) of Bi_2Se_3 nanoplates were irradiated by a NIR laser (808 nm, 1 W) for 5 min. The temperatures of the solutions were monitored by a thermocouple microprobe (φ = 0.5 mm) submerged in the solution in a 1-cm square cuvette. The probe was placed at such a position that the direct irradiation of the laser on the probe was avoided.

For the cell toxicity assay, H22 cells were precultured in 96-well cell culture plates (1×10^4 cells per well) for 24 h and then added with Bi_2Se_3 nanoplates at a series of concentrations. After incubation for 24 h, cells were rinsed with PBS and then were irradiated by the 808 nm laser at a power density of 1 W cm^{-2} for 5 min. After 24 h incubation, the standard MTT (Sigma) assay was carried out to determine the cell viabilities relative to the control untreated cells (incubated with the same volume of PBS).

In vivo photothermal therapy effects. The H22 tumor models were generated by subcutaneous injection of 1×10^6 H22 cells (Balb/c background) in PBS on the right rear flank of each mouse. The Bi_2Se_3 nanoplates were injected to the mice when the tumor volumes approached about 100 mm^3. For photothermal treatment, the mice of each group were intratumorally injected with 100 μl of each solution (1 mg ml^{-1} Bi_2Se_3 nanoplates solution or sterile water) and immediately irradiated with continuous NIR laser to tumor region for 5 min at the power density of 2 Wcm^{-2}. The tumor sizes were measured by a caliper every other day and were calculated using the equation (1): volume = $ab^2/2$, where a is the maximum diameter of tumor and b is the minimum diameter of tumor. Relative tumor volumes were calculated as V/V_0 (V_0 is the tumor volume when the treatment was initiated).

1. Cancer [homepage on the Internet]. Geneva: World Health Organization. Accessed January 15, 2013. Available from: http://www.who.int/cancer/about/facts/en/.
2. Funkhouser, J. Reinventing pharma: the theranostic revolution. *Curr. Drug Discovery* **2**, 17–19 (2002).
3. Bardhan, R., Lal, S., Joshi, A. & Halas, N. J. Theranostic nanoshells: from probe design to imaging and treatment of cancer. *Acc. Chem. Res.* **44**, 936–946 (2011).
4. Davis, M. E., Chen, Z. G. & Shin, D. M. Nanoparticle therapeutics: an emerging treatment modality for cancer. *Nat. Rev. Drug Discovery* **7**, 771–782 (2008).
5. Petros, R. A. & DeSimone, J. M. Strategies in the design of nanoparticles for therapeutic applications. *Nat. Rev. Drug Discovery* **9**, 615–627 (2010).
6. Dong, H. F. *et al.* Target-cell-specific delivery, imaging, and detection of intracellular microRNA with a multifunctional SnO_2 nanoprobe. *Angew. Chem. Int. Ed.* **51**, 4607–4612 (2012).
7. Lee, D. E. *et al.* Multifunctional nanoparticles for multimodal imaging and theragnosis. *Chem. Soc. Rev.* **41**, 2656–2672 (2012).
8. Xie, J., Liu, G., Eden, H. S., Ai, H. & Chen, X. Y. Surface-engineered magnetic nanoparticle platforms for cancer imaging and therapy. *Acc. Chem. Res.* **44**, 883–892 (2011).
9. Chen, T. *et al.* Smart multifunctional nanostructure for targeted cancer chemotherapy and magnetic resonance imaging. *ACS Nano* **5**, 7866–7873 (2011).
10. Reddy, L. H., Arias, J. L., Nicolas, J. & Couvreur, P. Magnetic nanoparticles: design and characterization, toxicity and biocompatibility, pharmaceutical and biomedical applications. *Chem. Rev.* **112**, 5818–5878 (2012).
11. Kostarelos, K., Bianco, A. & Prato, M. Promises, facts and challenges for carbon nanotubes in imaging and therapeutics. *Nat. Nanotechnol.* **4**, 627–633 (2009).

12. Kam, N. W. S., Connell, M. O., Wisdom, J. A. & Dai, H. Carbon nanotubes as multifunctional biological transporters and near-infrared agents for selective cancer cell destruction. *Proc. Natl Acad. Sci. USA* **102**, 11600–11605 (2005).
13. Xia, Y. N. *et al*. Gold nanocages: from synthesis to theranostic applications. *Acc. Chem. Res.* **44**, 914–924 (2011).
14. Huang, X. H., Neretina, S. & El-Sayed, M. A. Gold nanorods: from synthesis and properties to biological and biomedical applications. *Adv. Mater.* **21**, 4880–4910 (2009).
15. Ke, H. T. *et al.* Gold-nanoshelled microcapsules: a theranostic agent for ultrasound contrast imaging and photothermal therapy. *Angew. Chem. Int. Ed.* **50**, 3017–3021 (2011).
16. Hirsch, L. R. *et al.* Nanoshell-mediated near-infrared thermal therapy of tumors under magnetic resonance guidance. *Proc. Natl Acad. Sci. USA* **100**, 13549–13554 (2003).
17. Chen, Y. L. *et al.* Experimental realization of a three-dimensional topological insulator, Bi_2Te_3. *Science* **325**, 178–181 (2009).
18. Kong, D. S. & Cui, Y. Opportunities in chemistry and materials science for topological insulators and their nanostructures. *Nat. Chem.* **3**, 845–849 (2011).
19. Xia, Y. *et al*. Observation of a large-gap topological-insulator class with a single Dirac cone on the surface. *Nat. Phys.* **5**, 398–402 (2009).
20. Hor, Y. S. *et al*. *p*-type Bi_2Se_3 for topological insulator and low-temperature thermoelectric applications. *Phys. Rev. B* **79**, 195208 (2009).
21. LaForge, A. D. *et al*. Optical characterization of Bi_2Se_3 in a magnetic field: Infrared evidence for magnetoelectric coupling in a topological insulator material. *Phys. Rev. B* **81**, 125120 (2010).
22. Yu, Y., Sun, W. T., Hu, Z. D., Chen, Q. & Peng, L. M. Oriented Bi_2Se_3 nanoribbons film: structure, growth, and photoelectric properties. *Mater. Chem. Phys.* **124**, 865–869 (2010).
23. Sun, H. Z., Li, H. Y., Harvey, I. & Sadler, P. J. Interactions of bismuth complexes with metallothionein(II). *J. Biol. Chem.* **274**, 29094–29101 (1999).
24. Briand, G. G. & Burford, N. Bismuth compounds and preparations with biological or medicinal relevance. *Chem. Rev.* **99**, 2601–2657 (1999).
25. Rabin, O., Perez, J. M., Grimm, J., Wojtkiewicz, G. & Weissleder, R. An X-ray computed tomography imaging agent based on long-circulating bismuth sulphide nanoparticles. *Nat. Mater.* **5**, 118–122 (2006).
26. Kinsella, J. M. *et al.* X-ray computed tomography imaging of breast cancer by using targeted peptide-labeled bismuth sulfide nanoparticles. *Angew. Chem. Int. Ed.* **50**, 12308–12311 (2011).
27. Ai, K. L. *et al*. Large-scale synthesis of Bi_2S_3 nanodots as a contrast agent for in vivo X-ray computed tomography imaging. *Adv. Mater.* **23**, 4886–4891 (2011).
28. Whanger, P. D. Selenium and its relationship to cancer: an update. *Br. J. Nutr.* **91**, 11–28 (2004).
29. Rayman, M. P. The importance of selenium to human health. *Lancet* **356**, 233–241 (2000).
30. Rayman, M. P. Selenium in cancer prevention: a review of the evidence and mechanism of action. *Proc. Nutr. Soc.* **64**, 527–542 (2005).
31. Min, Y. *et al.* Quick, controlled synthesis of ultrathin Bi_2Se_3 nanodiscs and nanoplates. *J. Am. Chem. Soc.* **134**, 2872–2875 (2012).
32. Buhler, V. Kollidon® Polyvinylpyrrolidone for the Pharmaceutical Industry 9–125 (BASF Fine Chemicals, Ludwigshafen, 1998).
33. Sun, Y. G. & Xia, Y. N. Shape-controlled synthesis of gold and silver nanoparticles. *Science* **298**, 2176–2179 (2002).
34. Lu, G. *et al*. Imparting functionality to a metal-organic framework material by controlled nanoparticle encapsulation. *Nat. Chem.* **4**, 310–316 (2012).
35. Silverstein, S. C., Steinman, R. M. & Cohn, Z. A. Endocytosis. *Annu. Rev. Biochem.* **46**, 669–722 (1977).
36. Dreaden, E. C., Mackey, M. A., Huang, X. H., Kangy, B. & El-Sayed, M. A. Beating cancer in multiple ways using nanogold. *Chem. Soc. Rev.* **40**, 3391–3404 (2011).
37. Welsher, K. *et al*. A route to brightly fluorescent carbon nanotubes for near infrared imaging in mice. *Nat. Nanotechnol.* **4**, 773–780 (2009).
38. Yang, K. *et al.* In vitro and in vivo near-infrared photothermal therapy of cancer using polypyrrole organic nanoparticles. *Adv. Mater.* **24**, 5586–5592 (2012).
39. Zha, Z., Yue, X., Ren, Q. & Dai, Z. Uniform polypyrrole nanoparticles with high photothermal conversion efficiency for photothermal ablation of cancer cells. *Adv. Mater.* **25**, 777–782 (2013).
40. Cheng, L., Yang, K., Chen, Q. & Liu, Z. Organic stealth nanoparticles for highly effective in vivo near-infrared photothermal therapy of cancer. *ACS Nano* **6**, 5605–5613 (2012).
41. Yang, J. *et al.* Convertible organic nanoparticles for near-infrared photothermal ablation of cancer cells. *Angew. Chem. Int. Ed.* **50**, 441–444 (2011).
42. Moon, H. K., Lee, S. H. & Choi, H. C. In vivo near-infrared mediated tumor destruction by photothermal effect of carbon nanotubes. *ACS Nano* **3**, 3707–3713 (2009).
43. Ghosh, S. *et al.* Increased heating efficiency and selective thermal ablation of malignant tissue with DNA-encased multiwalled carbon nanotubes. *ACS Nano* **3**, 2667–2673 (2009).
44. Robinson, J. T. *et al.* High performance in vivo near-IR (>1 μm) imaging and photothermal cancer therapy with carbon nanotubes. *Nano Res.* **3**, 779–793 (2010).
45. Liu, X. *et al.* Optimization of surface chemistry on single-walled carbon nanotubes for in vivo photothermal ablation of tumors. *Biomaterials*, **32**, 144–151 (2011).
46. Robinson, J. T. *et al.* Ultrasmall reduced graphene oxide with high near-infrared absorbance for photothermal therapy. *J. Am. Chem. Soc.* **133**, 6825–6831 (2011).
47. Yang, K. *et al.* Graphene in mice: ultrahigh in vivo tumor uptake and efficient photothermal therapy. *Nano Lett.* **10**, 3318–3323 (2010).
48. Yang, K. *et al.* The influence of surface chemistry and size of nanoscale graphene oxide on photothermal therapy of cancer using ultra-low laser power. *Biomaterials*, **33**, 2206–2214 (2012).
49. Huang, X. Q. *et al.* Freestanding palladium nanosheets with plasmonic and catalytic properties. *Nat. Nanotechnol.* **6**, 28–32 (2011).
50. Chou, S. S. *et al.* Chemically exfoliated MoS_2 as near-infrared photothermal agents. *Angew. Chem. Int. Ed.* **52**, 4160–4164 (2013).
51. Zhou, M. *et al.* A chelator-free multifunctional [^{64}Cu]CuS nanoparticle platform for simultaneous micro-PET/CT imaging and photothermal ablation therapy. *J. Am. Chem. Soc.* **132**, 15351–15358 (2010).
52. Tian, Q. *et al.* Hydrophilic flower-like CuS superstructures as an efficient 980 nm laser-driven photothermal agent for ablation of cancer cells. *Adv. Mater.* **23**, 3542–3547 (2011).
53. Tian, Q. *et al.* Hydrophilic Cu_9S_5 nanocrystals: A photothermal agent with a 25.7% heat conversion efficiency for photothermal ablation of cancer cells in vivo. *ACS Nano* **5**, 9761–9771 (2011).
54. Hessel, C. M. *et al.* Copper selenide nanocrystals for photothermal therapy. *Nano Lett.* **11**, 2560–2566 (2011).

Acknowledgments

The authors gratefully acknowledge the financial from the National Basic Research Program of China (No. 2010CB732403), the National Natural Science Foundation of China (No. 21125524, No. 20975023), the Program for New Century Excellent Talents in University of China (09-0014), the Program for Changjiang Scholars and Innovative Research Team in University (No. IRT1116) and the National Science Foundation of Fujian Province (2010J06003).

Author contributions

H.H.Y. and G.N.C. supervised and directed the overall project. H.H.Y. and J.L. conceived and designed the experiments. J.L., F.J., B.Y. and D.R.C. contributed to the CT experiments and data interpretation. J.L., X.R.S., Y.L. and W.R.S. contributed to the photothermal therapy experiments. H.H.Y., J.L. and G.N.C. discussed the results and analysed the data and wrote the manuscript. All the authors were involved in the discussions.

Additional information

Supplementary information accompanies this paper at http://www.nature.com/scientificreports

Competing financial interests: The authors declare no competing financial interests.

How to cite this article: Li, J. *et al.* Topological insulator bismuth selenide as a theranostic platform for simultaneous cancer imaging and therapy. *Sci. Rep.* **3**, 1998; DOI:10.1038/srep01998 (2013).